Laser energy-pooling processes in an optically thick Cs vapor near a dissipative surface

Jean-Marie Gagné and Karine Le Bris

Laboratoire d'optique et de spectroscopie, Département de Génie Physique, École Polytechnique de Montréal, C.P. 6079, Succursale Centre-Ville, Montréal, Québec H3C 3A7, Canada

Marie-Claude Gagné

Stocker Yale Canada, Inc, 275 Kesmark, Dollard-des-Ormeaux, Québec H9B 3J1, Canada

Received March 27, 2002; revised manuscript received June 27, 2002

We characterize, for the first time to our knowledge, the laser-induced backward fluorescence (retrofluorescence) spectra that result from energy-pooling collisions between Cs atoms near a dissipative thin Cs layer on a glass substrate. We resolve, experimentally and theoretically, the laser spectroscopic problem of energy-pooling processes related to the nature of the glass–metallic vapor interface. Our study focused on the integrated laser-induced retrofluorescence spectra for the 455.5-nm ($7^2P_{3/2}$–$6^2S_{1/2}$) and 852.2-nm ($6^2P_{3/2}$–$6^2S_{1/2}$) lines as a function of laser scanning through pumping resonance at the 852.2-nm line. We experimentally investigate the retrofluorescence from 420 to 930 nm, induced by a diode laser tuned either in the wings or in the center of the pumping resonance line. We present a detailed theoretical model of the retrofluorescence signal based on the radiative transfer equation, taking into account the evanescent wave of the excited atomic dipole strongly coupled with a dissipative surface. Based on theoretical and experimental results, we evaluate the effective nonradiative transfer rate $\bar{A}^f_{6^2P_{3/2}\rightarrow 6^2S_{1/2s}}$ for atoms in the excited $6^2P_{3/2}$ level located in the near-field region of the surface of the cell. Values extracted from the energy-pooling process analysis are equivalent to those found directly from the 852.2-nm resonance retrofluorescence line. We show that the effective energy-pooling coefficients $\tilde{k}_{7^2P_{3/2}}$ and $\tilde{k}_{7^2P_{1/2}}$ are approximately equal. The agreement between theory and experiment is remarkably good, considering the simplicity of the model. © 2002 Optical Society of America

OCIS codes: 020.2070, 240.6490, 290.2200, 300.2530, 300.6490, 350.2450.

1. INTRODUCTION

The monochromatic semiconductor tunable laser has been used extensively for both fundamental and applied work on vapor in glass cells. In particular, the linear spectral effects related to laser photon absorption, laser-induced fluorescence, or laser cooling in optically thin vapor are well known. For optically thick vapor, the spectrophysics problems are totally different. Characteristic features of the spectroscopic effects related to laser-light interaction with vapor are often problematic and lead to new challenges. The laser-induced effects in an optically thick vapor are more numerous and richer than those from an optically thin vapor. Obviously, the features are complex because the laser beam and the atoms interact in the close vicinity of the surface cell, which can act as a dissipative surface. This kind of physical environment strongly alters the atomic response to resonance interaction light and spontaneous emission. The spectroscopic phenomena that result from monochromatic laser irradiation could happen either in a deep vapor volume (far-field region) or in a boundary vapor layer (near-field region) adjacent, in the case of metallic vapor, to a surface that is dissipative because of the adsorption of metallic atoms onto the internal surface of the glass cell. Their interpretation requires our understanding of surface science (atoms lost to the wall through physisorption and chemisorption), of atomic dynamic processes, and of the spontaneous emission and scattering of resonance photons toward the surface. Experimental and theoretical investigations of these effects continue to be fundamental and important subjects of laser spectrophysics research.

Conventional surface analytic methods and traditional linear laser absorption or laser-induced fluorescence spectroscopy are not suitable for the investigation of laser-induced excited atomic effects in optically thick metallic vapor near a dissipative surface. Many physical aspects must be understood: vapor density of ground-state and excited-state atoms, atomic reactions with the cell surface, photon-trapping effects, and backward radiance from the interface. Physical properties of the surface and the evolution of the laser beam intensity as it penetrates the vapor are most important for determination of the nature of laser-induced effects at the interface. Nonradiative transfer rates, as well as combined effects of radiation and migration of excited atoms, also affect the behavior of the irradiated interface.

Only a few, nonconventional, laser spectroscopy methods are suitable for the investigation of optical properties of a dense excited atomic metallic vapor near a dissipative surface: selective reflection spectroscopy,[1] evanescent wave spectroscopy,[2,3] and laser retrofluorescence spectroscopy.[4] Each method has its advantages. The se-

lective reflection technique is particularly suitable for the study of long-range atom–wall interactions and collision-induced broadening. Evanescent wave spectroscopy has been used for the investigation of collisional dynamics of the atoms and for determination of the density of alkali metal vapor in the vicinity of the surface.

In a recent paper,[4] laser retrofluorescence spectroscopy was shown to characterize efficiently the nonradiative transfer of the energy of excited atoms to the dissipative surface. In this paper we focus on the characterization of the laser-induced retrofluorescence spectrum related to energy-pooling processes $\mathrm{Cs}(6^2P_{3/2}) + \mathrm{Cs}(6^2P_{3/2})$ stimulated by a tunable diode laser near a dissipative film on a glass substrate. To our knowledge, theoretical and experimental laser retrofluorescence spectra over a large spectral range have not been investigated previously. The interpretation of correlation inhibition effects between resonance and nonresonance retrofluorescence spectra is unknown. This lack of information motivated us to perform fundamental experimental investigations and a theoretical analysis of this problem. Following the introduction, in Section 2 we begin by recalling the main properties of energy-pooling processes between two identical excited $\mathrm{Cs}(6^2P_{3/2})$ atoms. We then model the laser-induced retrofluorescence spectrum that results from energy-pooling processes, taking into account the evanescent wave of the excited atomic dipoles strongly coupled with a dissipative surface when the excited atom is located in near-field region. In Section 3 we derive a theoretical expression for the laser-induced retrofluorescence signal. In Section 4 we present the experimental retrofluorescence results that we quantitatively compare in Section 5 with our theoretical results. We calculate the effective nonradiative transfer rate of the $6^2P_{3/2}$ level in the near-field region. Energy-pooling coefficients are evaluated.

2. REVIEW OF THE ENERGY-POOLING PROCESSES BETWEEN TWO EXCITED Cs ($6^2P_{3/2}$) ATOMS

A major objective of this paper is the investigation of energy-pooling processes under continuous optical pumping with the 852.2-nm line in the linear regime, when the excited atoms are in close proximity to a dissipative film. The aim of this brief review is to give a descriptive summary of the pertinent characteristic properties of energy-pooling collisions of two excited $\mathrm{Cs}(6^2P_{3/2})$ atoms, leading to the production of highly excited atomic states.

Numerous experiments have been reported about the behavior of Cs metal vapor after irradiation with continuous laser light power of ~500 mW, tuned to the absorption transition $\mathrm{Cs}(6^2S_{1/2}) \rightarrow \mathrm{Cs}(6^2P_{3/2})$. Pooling effects occur under relatively low vapor density (10^{12} at. cm^{-3}) without interface effects. The reaction is in the form

$$\mathrm{Cs}\ (6^2P_J) + \mathrm{Cs}\ (6^2P_{J'}) \rightarrow \mathrm{Cs}\ (nl_{J''}) + \mathrm{Cs}\ (6^2S_{1/2}), \tag{1}$$

where $\mathrm{Cs}(nl_{J''})$ denotes a highly excited atom, J and J' are equal to 3/2 or 1/2, n is the total quantum number, l is the angular momentum of the electron in its orbit, and J'' is the total angular momentum.

This pooling reaction requires the existence of resonance at a value between the total energies (including the kinetic energy) of the interacting partners. Particularly when the partners have the same excitation energy, this requirement leads to doubling the energy of the initial state of one of the partners within the limit of ΔE_c, the difference between the total kinetic energy before and after the collision. In saturated Cs vapor, this process leads to several highly excited states described in reaction (1) by the quantum numbers n, l, and J''.

To obtain an appropriate quantitative interpretation of the complex retrofluorescence spectra arising from the reactions, a number of simultaneous processes have to be considered. These processes depend on the temperature and atomic density, the laser-light intensity, and the environment of the excited atoms, as we shall see in Section 3, in which we introduce a nearby dissipative layer.

When the laser intensity is tuned to the absorption line at 852.2 nm, we inevitably identify three entrance channels for energy-pooling processes: $6^2P_{1/2} + 6^2P_{3/2}$, $6^2P_{1/2} + 6^2P_{1/2}$, and $6^2P_{3/2} + 6^2P_{3/2}$ since, from the traditional interpretation of sensitized fluorescence (i.e., fluorescence from the 6^2P_J level that is not pumped by the laser), fine-structure changing collisions of the second kind,

$$\mathrm{Cs}\ (6^2P_{3/2}) + \mathrm{Cs}\ (6^2S_{1/2}) \leftrightarrow \mathrm{Cs}\ (6^2P_{1/2}) + \mathrm{Cs}\ (6^2S_{1/2}), \tag{2}$$

result in the population of both levels. Evidently, in some specific cases determined by the vapor density, we must consider the hyperfine structure $6^2P_{3/2}$ ($F_e = 5, 4, 3, 2$) and $6^2S_{1/2}$ ($F_g = 4, 3$), where F_e and F_g are quantum numbers. In these cases, we can have a spectral sub-Doppler effect.

The large fine structure of the $6^2P_{3/2}$–$6^2P_{1/2}$ state and the important hyperfine structure of $6^2P_{3/2}(F_e)$ make the study of energy-pooling collisions more complicated. However, the hyperfine structure can be used to characterize the dynamic phenomena and to permit the identification of spontaneous hyperfine transition.

Figure 1 shows a schematic diagram of the most important Cs energy levels involved in the pooling process: the horizontal dashed line represents a virtual level lying at twice the $6^2P_{3/2}$ level energy. The broken upward arrows ($8^2S_{1/2}$, 4^2F_J) show endothermic reactions whereas the broken downward arrows correspond to exothermic collision (7^2P_J, 6^2D_J). Solid downward arrows indicate radiative transitions that result from pooling fluorescence levels. In the fluorescence spectral range between 925 and 450 nm, seven spontaneous emission transitions are classified, if we do not consider the 852.2-nm resonance line and the 894-nm sensitized line. The latter is an important special transition that is to be discussed elsewhere because the traditional interpretation of this line does not result from the pooling process. The population density in the excited state 7^2P is proportional to the square of the number density of excited 6^2P atom pairs in the vapor volume and the energy-pooling rate coefficient connected to different entrance channels and the effective

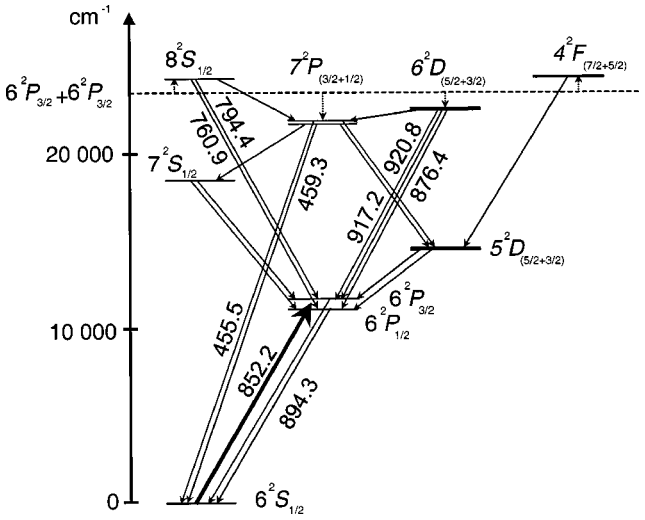

Fig. 1. Spectrum wavelength and lower excited levels of the Cs atom that we studied. Wavelengths are given in nanometers. The populations in the high-lying levels are attributed to excited-atoms–excited atom collisions in which two atoms pool their internal energy to produce a ground-state atom and one in a more highly excited level. Solid downward arrows represent radiative transition and broken arrows represent collisional processes.

lifetime of the 7^2P_J state. Since the population of 7^2P_J is governed by the 6^2P_J population density, we must observe an important mutual relationship between them. The nonradiative energy transfer between excited atoms 6^2P_J and 7^2P_J in the vapor necessarily affects the number density in the excited 7^2P_J atomic level. The fluorescence or retrofluorescence spectra resulting from the energy-pooling collision will have an important link with nonradiative processes. We expect all atomic spectral line intensities that result from energy-pooling collisions to be strongly influenced by nonradiative processes. Detailed knowledge of the density and spatial distribution of the excited atoms in the volume of the vapor are required for a quantitative interpretation of the fluorescence and retrofluorescence spectra. The rate equation for the population of the 7^2P_J level has been extensively studied by de Tomasi *et al.*[5] The atomic density in the excited 6^2P_J state has been modeled.

In Section 3 we use the preceding information for modeling the retrofluorescence signal dominated by energy pooling of 2Cs $(6^2P_{3/2})$ in an optically thick saturated vapor in the close vicinity of a thin metallic layer.

3. MODELING OF THE RETROFLUORESCENCE SIGNAL RELATED TO THE ENERGY-POOLING PROCESS Cs $(6^2P_{3/2})$ + Cs $(6^2P_{3/2})$

In this section we present a simple model of the retrofluorescence signals produced by the energy-pooling collisions at the glass–atomic-vapor interface. We analyze the evolution of a weak, parallel monochromatic laser beam that passes through the near- and the far-field regions of the interface. The interface is composed of an adsorbate-covered surface and a slow penetration of Cs into the glass surface underneath, forming a thin boundary dissipative layer. Between this layer and the reservoir of Cs vapor, we consider a near-field region. In this wavelength thickness layer, the evanescent waves of the excited atomic dipoles are strongly coupled with the metallic surface (Chance *et al.*[6]). The near-field region contains a great number of atoms in the ground state $(7.72 \times 10^{13}$ at. cm^{-3} at 130 °C) uniformly distributed over the volume. The surface and the atoms located in the near-field region constitute an efficient resonant dissipative environment with maximum dissipation at the center resonance line. This arrangement and interrelationship is considered to be an elementary transformer of photonic energy into thermal energy. Our model for the retrofluorescence energy-pooling process takes into account the nonradiative phenomena that are due to the elementary mechanism of photonic energy transformation. The spectral signature of the atomic spontaneous emission that is due to this mechanism is indicated by deep dips in the retrofluorescence energy-pooling collision spectra. All the atomic lines related to the energy-pooling process have this nonradiative relaxation signature, particularly at the centerline.

The energy-pooling process in a thick Cs vapor near the dissipative thin layer studied in this section is limited to the reaction

$$\begin{aligned} 2\mathrm{Cs}\ (6^2P_{3/2}) &\rightarrow \mathrm{Cs}\ (7^2P_J) + \mathrm{Cs}\ (6^2S_{1/2}) \\ &\rightarrow 2\mathrm{Cs}\ (6^2S_{1/2}) \\ &\quad + h\nu(455.5 \text{ and } 459.3 \text{ nm}). \end{aligned} \tag{3}$$

This reaction is a good candidate for the modeling and measurement of the retrofluorescence signal because the reaction has been extensively studied by de Tomasi *et al.*[5] and by Jabbour *et al.*[7] and because the spectral lines at 455.5 and 459.3 nm are easily experimentally observed, as we shall see in Section 4.

In formulating our model, we must consider the hyperfine structure of the absorbing Cs transition $[6^2S_{1/2} \rightarrow 6^2P_{3/2}]$. Focusing our attention on reaction (3) allows us to eliminate a number of transitions and levels in Fig.

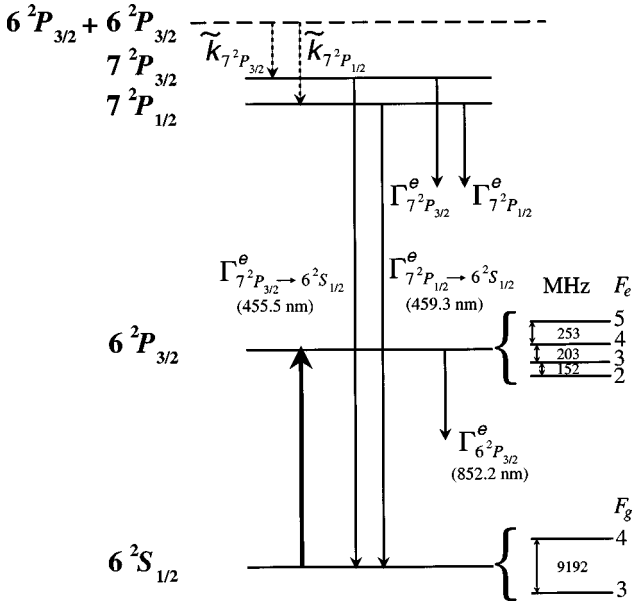

Fig. 2. Schematic of the energy level diagram of Cs.

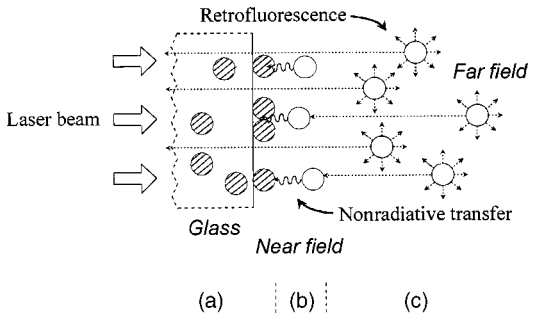

Fig. 3. Physical description of the characteristic region of the window cell: (a) glass substrate with adsorbed Cs atoms, (b) interface region where Cs atoms interact strongly with the surface, (c) region of free atoms.

1 to obtain the simplified schematic presented in Fig. 2, which shows a schematization of these hyperfine levels for the Cs ($6^2S_{1/2}$) and Cs ($6^2P_{3/2}$) terms. These atomic terms are composed of two hyperfine Cs ($6^2S_{1/2}$, $F_g = 3$ or 4) ground levels energetically isolated from each other by a gap of 9.193 GHz and four excited lying hyperfine Cs ($6^2P_{3/2}$, $F_e = 2, 3, 4$ and 5) levels over a spectral interval of 604 MHz. Considering both the collisions and the distribution of the kinetic energy in the saturated vapor, it is reasonable for us to assume a complete redistribution of the excited population. In this representation we limit ourselves to the observation of the signals at 455.5 nm [$7^2P_{3/2} \rightarrow 6^2S_{1/2}$] and 459.3 nm [$7^2P_{1/2} \rightarrow 6^2S_{1/2}$]. We neglect fine structure $6^2P_{3/2} + 6^2P_{1/2}$ and $6^2P_{1/2} + 6^2P_{1/2}$ mixing collisions when the monochromatic laser is tuned to 852.2 nm [$6^2S_{1/2} \rightarrow 6^2P_{3/2}$]. The radiative transitions in the far-field region are represented by downward straight arrows. $\Gamma^e_{7^2P_J}$ is the sum of the Einstein spontaneous emission rates for transitions to all lower levels in the absence of photon trapping and quenching collisions. $\Gamma^e_{7^2P_J \rightarrow 6^2S_{1/2}}$ is the effective radiative rate for level 7^2P_J to level $6^2S_{1/2}$. $\tilde{k}_{7^2P_J}$ represents effective energy-pooling coefficients ($J = 3/2,1/2$). If the 7^2P_J signals in the 852.2-nm pumping were due to both 6^2D and 8^2S cascades, we would expect to see $7^2P_{3/2} \rightarrow 6^2S_{1/2}$ fluorescence signals twice as large as the $7^2P_{1/2} \rightarrow 6^2S_{1/2}$ signals. Experimentally, this is not the case, as we shall see in Section 4.

Nevertheless, in the situation in which the 7^2P_J population is due primarily to the $8^2S \rightarrow 7^2P$ cascade, we would have

$$\tilde{k}_{7^2P_J} = \tilde{k}^{(3/2)}_{7^2P_J} + \frac{\Gamma^e_{8^2S_{1/2} \rightarrow 7^2P_J}}{\Gamma^e_{8^2S_{1/2}}} \tilde{k}^{(3/2)}_{8^2S_{1/2}}, \qquad (4)$$

where $\tilde{k}^{(3/2)}_{7^2P_j, 8^2S_{1/2}}$ are the effective rate coefficients for the 7^2P_J and $8^2S_{1/2}$ energy-pooling process levels. The broken arrows in Fig. 2 represent collision processes, F_e is the hyperfine quantum number for the $6^2P_{3/2}$ excited level and F_g is for the $6^2S_{1/2}$ ground level.

We must also consider collisional mixing among structural and collisional excitation transfer processes such as $6^2D + M \leftrightarrow 7^2P + M$, where M is the ground state of Cs or of an impurity diatomic molecule in the vapor. Such processes can distort the apparent energy-pooling rate coefficients. We can estimate the collisional mixing of the $6^2P_{3/2} + 6^2S_{1/2} \rightarrow 6^2P_{1/2} + 6^2S_{1/2}$ fine structure by analyzing the ratio of the sensitized fluorescence to the direct fluorescence. The values of the measured ratios cannot be explained only by $6^2P_{3/2} + 6^2S_{1/2}$ collisions, a discrepancy that will be discussed in a subsequent paper. Nevertheless, Fig. 2 presents a reasonable schematization of the atomic levels when the observation is limited to the retrofluorescence signal related to the $7^2P_J \rightarrow 6^2S_{1/2}$ spontaneous emission lines.

In our modeling of the retrofluorescence signal, we used the physical and geometric description of the characteristic region of the cell developed by Le Bris *et al.*[4] (see Fig. 3). A substantial amount of Cs diffuse inside and adsorbs on glass surface (a). Between this thin metallic layer structure and the reservoir of Cs vapor, we consider a so-called near-field region (b) or a vapor boundary layer. The excited atoms in this boundary layer are especially sensitive to the immediate thin metallic layer surface. This arrangement is described as a spectral optical filter. We assume that each laser photon and $7^2P_J \rightarrow 6^2S_{1/2}$ emission photon absorbed by an atom located in this region is quickly transformed into thermal energy. The far-field region (c) corresponds to the infinitely extended free atoms adjacent to the near-field structure. In this region, excited 6^2P_J, 7^2P_J, $8^2S_{1/2}$, 6^2D_J,... atoms do not interact with the thin metallic film. The laser energy-pooling processes are especially important in this region for the generation of line retrofluorescence signals. The far-field region therefore becomes a light source observable through the window in the opposite direction with respect to the laser beam.

The relevant geometric parameters are indicated in Fig. 4. $\overline{x_f}$ is the mean geometric depth of the near-field region adjacent to the thin dissipative layer. The intensity of the laser beam, $F_{\nu_L}(\mathrm{W/cm^2})$, is sufficiently weak to ensure that the number of excited atoms, $|e\rangle$ remains much less than the number that remains in the ground state, $|g\rangle$. $L^J(\nu_L, F_g)$ is the integrated retrofluorescence radiance associated with the lines from the energy-pooling processes observed at the origin $x = 0$ (entrance window). In an elementary slice of vapor of thickness dx

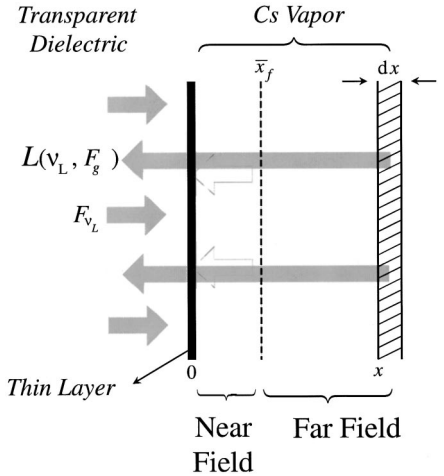

Fig. 4. Geometric description of the characteristic region of the window cell.

located in the far-field region at a distance x from the entrance window, excited atoms at the 7^2P_J level, are created only by 2Cs $(6^2P_{3/2})$ energy-pooling collisions. $n_{7^2P_J}(x,\ \nu_L,\ F_g)$, the population density of the 7^2P_J levels, is related to the laser frequency ν_L, the spectral optical filtering effect, the effective energy-pooling coefficients $\tilde{k}_{7^2P_J}$, the effective transition rates, and photon-trapping rate. To simplify the formulation, we neglect reflection, absorption, and scattering of the energy laser beam in the glass window and on the thin boundary layer on the glass.

The spectral radiance $L^J_{\nu,x}(\nu_L,\ F_g)$ at $x = 0$ that corresponds to the $7^2P_J \rightarrow 6^2S_{1/2}$ transition from an elementary slice of vapor of thickness dx located at x, where only the self-absorption process is considered, is given by

$$\begin{aligned} L^J_{\nu,x}(\nu_L,\ F_g) &= \frac{h\nu}{2}\Gamma^e_{7^2P_J\rightarrow 6^2S_{1/2}}\alpha^l_{7^2P_J\rightarrow 6^2S_{1/2}} \\ &\times \exp[-\bar{\tau}^f_{6^2S_{1/2}\rightarrow 7^2P_J}(\nu)]n_{7^2P_J}(x,\ \nu_L,\ F_g) \\ &\times \exp[-\bar{k}^l_{6^2S_{1/2}\rightarrow 7^2P_J}(\nu)x], \end{aligned} \tag{5}$$

where $\bar{\tau}^f_{6^2S_{1/2}\rightarrow 7^2P_J}(\nu)$ is the effective spectral optical thickness of the stop-band filter at frequency ν, $\alpha^l_{7^2P_J\rightarrow 6^2S_{1/2}}$ is the normalized emission shape in the far-field region, $\bar{k}^l_{6^2S_{1/2}\rightarrow 7^2P_J}(\nu)$ is the effective spectral absorption for the $6^2S_{1/2}\rightarrow 7^2P_J$ transition line, and $\Gamma^e_{7^2P_J\rightarrow 6^2S_{1/2}}$ is the effective radiative rate for the $7^2P_J \rightarrow 6^2S_{1/2}$ transition line.

The rate equation for the density in the 7^2P_J level at x populated through the 2Cs $(6^2P_{3/2})$ energy-pooling collision is given by

$$\begin{aligned} \frac{\mathrm{d}}{\mathrm{d}t}n_{7^2P_J}(x,\ \nu_L,\ F_g) &= \frac{\tilde{k}_{7^2P_J}}{2}n^2_{6^2P_{3/2}}(x,\ \nu_L,\ F_g) \\ &- \Gamma^e_{7^2P_J}n_{7^2P_J}(x,\ \nu_L,\ F_g), \end{aligned} \tag{6}$$

where $n_{6^2P_{3/2}}(x,\ \nu_L,\ F_g)$ is the population density in the $6^2P_{3/2}$ level following the pumping resonance transition. The steady-state rate equation has the solution

$$n_{7^2P_J}(x,\ \nu_L,\ F_g) = \frac{\tilde{k}_{7^2P_J}}{2}(\Gamma^e_{7^2P_J})^{-1}n^2_{6^2P_{3/2}}(x,\ \nu_L,\ F_g). \tag{7}$$

The rate equation for the density population at the level $6^2P_{3/2}$ level is described by the equation

$$\begin{aligned} \frac{\mathrm{d}n_{6^2P_{3/2}}(x,\ \nu_L,\ F_g)}{\mathrm{d}t} &= \frac{\mathrm{d}F_x(\nu_L)}{h\nu_L} - \Gamma^e_{6^2P_{3/2}}n_{6^2P_{3/2}}(x,\ \nu_L,\ F_g), \end{aligned} \tag{8}$$

where $\mathrm{d}F_x(\nu_L)$ is the rate of laser energy dissipated in an elementary slice of vapor located at x.

For steady pumping we have

$$n_{6^2P_{3/2}}(x,\ \nu_L,\ F_g) = \frac{\mathrm{d}F_x(\nu_L)}{h\nu_L\Gamma^e_{6^2P_{3/2}}}. \tag{9}$$

From le Bris *et al.*,[4] $\mathrm{d}F_x(\nu_L)$ is given by

$$\begin{aligned} \mathrm{d}F_x(\nu_L) = -F_{\nu_L}\sum_{F_e}\bar{k}^l_{F_g\rightarrow F_e}(\nu_L)\exp\left[-\sum_{F_e}\bar{\tau}^f_{F_g\rightarrow F_e}(\nu_L)\right] \\ \times \exp\left[-\sum_{F_e}\bar{k}^l_{F_g\rightarrow F_e}(\nu_L)x\right], \end{aligned} \tag{10}$$

where $\bar{k}^l_{F_g\rightarrow F_e}(\nu_L)$ is the effective spectral absorption coefficient of the saturated vapor located in the far-field region; $\bar{\tau}^f_{F_g\rightarrow F_e}(\nu_L)$ is the effective spectral optical thickness of the stop-band filter for the atomic hyperfine transition between the ground hyperfine level $|F_g\rangle$ and the excited level $|F_e\rangle$, respectively; and F_e and F_g are the hyperfine quantum numbers of the excited and ground levels. We related $\bar{k}^l_{F_g\rightarrow F_e}(\nu_L)$ and $\bar{\tau}^f_{F_g\rightarrow F_e}(\nu_L)$ to the atomic parameters (Le Bris *et al.*[4]) as

$$\bar{k}^l_{F_g\rightarrow F_e}(\nu_L) = \frac{\lambda^2}{8\Pi}\frac{2J_e+1}{2J_g+1}A_{J_e\rightarrow J_g}\bar{n}_{F_g}g_{F_eF_g}\alpha^l_{F_g\rightarrow F_e}(\nu_L), \tag{11}$$

$$\begin{aligned} \bar{\tau}^f_{F_g\rightarrow F_e}(\nu_L) &= \frac{\lambda^2}{8\pi}\frac{2J_e+1}{2J_g+1}\bar{A}^f_{F_e\rightarrow F_g}\bar{n}_{F_g}\bar{x}_f g_{F_eF_g}\alpha^f_{F_e\rightarrow F_e}(\nu_L), \end{aligned} \tag{12}$$

$$\bar{A}^f_{F_e\rightarrow F_g} = A_{J_e\rightarrow J_g}\bar{\varepsilon}_{F_g}g_{F_eF_g}, \tag{13}$$

$$g_{F_eF_g} = \frac{(2F_e+1)(2F_g+1)}{(2I+1)}\{\ldots 6j\ldots\}^2, \tag{14}$$

where $\bar{n}_{F_g}$ is the mean number density of the ground hyperfine level $|F_g\rangle$, a well-known function of temperature T,[8] $\alpha^l_{F_g\rightarrow F_e}(\nu_L)$ is the normalized absorption shape for each hyperfine line in the far-field region, $A_{J_e\rightarrow J_g}$ is the Einstein spontaneous emission between two degenerate levels whose statistical weights are $(2J_e+1)$ and $(2J_g+1)$, $\bar{A}^f_{F_e\rightarrow F_g}$ is the effective nonradiative transfer rate between $|F_e\rangle\rightarrow|F_g\rangle$ levels in the near-field region, I is the nucleus spin, $\{\ldots 6j\ldots\}$ is the symbol $6j$, and $\bar{\varepsilon}_{F_g}$ is the ratio between nonradiative and radiative transfer rates for the $6^2P_{3/2} \rightarrow 6^2S_{1/2}(F_g)$ transition.

The effective nonradiative transfer rate between $J_e \rightarrow J_g$ for atoms located in the near-field region is given by

$$\bar{A}^f_{J_e\rightarrow J_g} = \sum_{F_e}\sum_{F_g}\bar{A}^f_{F_e\rightarrow F_g} = A_{J_e\rightarrow J_g}\sum_{F_e}\sum_{F_g}\bar{\varepsilon}_{F_g}g_{F_eF_g}. \tag{15}$$

The signal $\phi_J(\nu_L,\ F_g)$ is proportional to the integrated radiance $L^J(\nu_L,\ F_g)$ evaluated at $x = 0$:

$$\phi_J(\nu_L,\ F_g) \propto L^J(\nu_L,\ F_g) = \int_{\Delta\nu}\int_0^{+\infty}L^J_{\nu,x}(\nu_L,\ F_g)\mathrm{d}x\mathrm{d}\nu, \tag{16}$$

Considering Eqs. (5), (7), (9), and (10), Eq. (16) becomes

$$\phi_J(\nu_L, F_g) \propto \frac{F_{\nu_L}^2 \Gamma^e_{7^2P_J\to 6^2S_{1/2}} \tilde{k}^l_{7^2P_J}}{(\Gamma^e_{6^2P_{3/2}})^2 \Gamma^e_{7^2P_J}} \left\{ \sum_{F_e} [\bar{k}^l_{F_g\to F_e}(\nu_L)] \right\}^2 \times \exp\left[-2 \sum_F \bar{\tau}^f_{F_g\to F_e}(\nu_L) \right] \Theta_{7^2P_J\to 6^2S_{1/2}}(\nu_L), \tag{17}$$

where $\Theta_{7^2P_J\to 6^2S_{1/2}}(\nu_L, F_g)$ is given by

$$\Theta_{7^2P_J\to 6^2S_{1/2}}(\nu_L, F_g) = \int \frac{\alpha^l_{7^2P_J\to 6^2S_{1/2}}(\nu) \exp[-\bar{\tau}^f_{6^2S_{1/2}\to 7^2P_J}(\nu)]}{\bar{k}^l_{6^2S_{1/2}\to 7^2P_J}(\nu) + 2 \sum_{F_e} \bar{k}^l_{F_g\to F_e}(\nu_L)} \mathrm{d}\nu. \tag{18}$$

It is clear from relation (17) and Eq. (18) that the signal ϕ_J is principally related to $\bar{k}^l_{F_g\to F_e}(\nu_L)$ and $\bar{\tau}^f_{F_g\to F_e}(\nu_L)$ for the $6^2S_{1/2}(F_g)\to 6^2P_{3/2}(F_e)$ resonance transition, and $\Theta_{7^2P_J\to 6^2S_{1/2}}(\nu_L)$ is a function of the atomic parameters for the $6^2S_{1/2}(F_g)\to 6^2P_{3/2}(F_e)$ and $7^2P_J\to 6^2S_{1/2}$ resonance transitions. The factor 2 in the transfer filter function is normal because $n_{7^2P_J} \propto n^2_{6^2P_{3/2}}$.

However, the right-hand side of relation (17) is a function too complex to analyze analytically. We can simplify it with a reasonable assumption. If we have

$$\bar{k}^l_{6^2S_{1/2}\to 7^2P_J}(\nu) \ll 2 \sum_{F_e} \bar{k}^l_{F_g\to F_e}(\nu_L), \tag{19}$$

the normalized $\phi^n_J(\nu_L, F_g)$ signal becomes

$$\phi^n_J(\nu_L, F_g) = \sum_{F_e} g_{F_eF_g} \alpha^l_{F_g\to F_e}(\nu_L) \times \exp\left[-2 \sum_{F_e} \bar{\tau}^f_{F_g\to F_e}(\nu_L) \right]. \tag{20}$$

Equation (20) can be used to obtain a hyperfine analytical normalized signal directly related to the energy-pooling collision process. $\phi^n_J(\nu_L, F_g)$ is determined only by atomic parameters related to the hyperfine structure of the $6^2S_{1/2}(F_g)\to 6^2P_{3/2}(F_e)$ transition. When the ground hyperfine levels overlap, Eq. (20) becomes

$$\phi^n_J(\nu_L) = \sum_{F_g} \sum_{F_e} g_{F_eF_g} \alpha^l_{F_g\to F_e}(\nu_L) \times \exp\left[-2 \sum_{F_g} \sum_{F_e} \bar{\tau}^f_{F_g\to F_e}(\nu_L) \right]. \tag{21}$$

With Eq. (20) we could evaluate the nonradiative transfer rate $\bar{A}^f_{F_e\to F_g}$ or $\bar{\varepsilon}_{F_g}$ between $|F_e\rangle \to |F_g\rangle$ in the near-field region. The same nonradiative transfer rate values are obtained equally from the signal of the 852.2-nm resonance line.

For illustration purposes, we consider the $6^2S_{1/2}$ $(F_g = 4) \to 6^2P_{3/2}$ $(F_e = 5, 4, 3)$ transition. In this case, we have

$$\sum_{F_e} g_{F_eF_g} \alpha^i_{F_g=4\to F_e}(\nu_L) = g_{34}\alpha^i_{43}(\nu_L, \bar{\nu}_{43}, \gamma^i_G, \gamma^i_{\mathcal{L}}) + g_{44}\alpha^i_{44}(\nu_L, \bar{\nu}_{43} - \alpha, \gamma^i_G, \gamma^i_{\mathcal{L}}) + g_{54}\alpha^i_{45}(\nu_L, \bar{\nu}_{43} - b, \gamma^i_G, \gamma^i_{\mathcal{L}}), \tag{22}$$

where $\alpha^i(\ldots)$ is a Voigt general formula where $i = l$ or f, $g_{34} = 0.159/2.908$, $g_{44} = 0.477/2.908$, $g_{54} = 1/2.908$, $a = 0.203$ GHz, $b = 0.456$ GHz, and γ^i_G is the full width at half-maximum (FWHM) of the Gaussian shape, and $\gamma^i_{\mathcal{L}}$ is the FWHM of the Lorentzian shape. The Doppler effect is dominant for the center of the line and the Lorentz line contribution for the edges. Using a parametric adjustment between experimental signal and theoretical values $\phi^n_J(\nu_L, F_g = 4)$, we estimate the important parameter $\bar{\varepsilon}_{F_g=4}$. Repeating this procedure for the $|F_g = 3\rangle \to |F_e = 4, 3, 2\rangle$ transition we get the complementary value $\bar{\varepsilon}_{F_g=3}$. Using both values of $\bar{\varepsilon}_{F_g=4 \text{ or } 3}$, we calculate $\bar{A}^f_{J_e\to J_g}$ by using the expression

$$\bar{A}^f_{J_e\to J_g} = \frac{A_{J_e\to J_g}}{16}(9\bar{\varepsilon}_{F_g=4} + 7\bar{\varepsilon}_{F_g=3}). \tag{23}$$

The Voigt profile cannot be expressed in a simple form, but must be evaluated by numerical integration.

When the pumping laser is tuned to $6^2S_{1/2} \to 6^2P_{3/2}$, as we have seen, both the 6^2D and 8^2S cascades could contribute to the $7^2P_{3/2} \to 6^2S_{1/2}$ and $7^2P_{1/2} \to 6^2S_{1/2}$ signals. We work with a vapor temperature higher than 85 °C, and we measure the $7^2P_J \to 6^2S_{1/2}$ ratio retrofluorescence signals with high precision. This has motivated us to estimate the ratio of the $\phi_{455.5\text{ nm}}(\nu_L)$ and $\phi_{459.3\text{ nm}}(\nu_L)$ signals by use of our model. The value of $\phi_{455.5\text{ nm}}(\nu_L)/\phi_{459.3\text{ nm}}(\nu_L)$ is given by

$$\frac{\phi_{455.5\text{ nm}}(\nu_L)}{\phi_{459.3\text{ nm}}(\nu_L)} = \frac{\Gamma^e_{7^2P_{3/2}\to 6^2S_{1/2}} \Gamma^e_{7^2P_{1/2}} \tilde{k}_{7^2P_{3/2}} \Theta_{455.5\text{ nm}}}{\Gamma^e_{7^2P_{1/2}\to 6^2S_{1/2}} \Gamma^e_{7^2P_{3/2}} \tilde{k}_{7^2P_{1/2}} \Theta_{459.3\text{ nm}}}, \tag{24}$$

where

$$\frac{\Theta_{455.5\text{ nm}}}{\Theta_{459.3\text{ nm}}} = \frac{\int_{\Delta\nu} \alpha^l_{7^2P_{3/2}\to 6^2S_{1/2}}(\nu) \exp[-\bar{\tau}^f_{6^2S_{1/2}\to 7^2P_{3/2}}(\nu)] \mathrm{d}\nu}{\int_{\Delta\nu} \alpha^l_{7^2P_{1/2}\to 6^2S_{1/2}}(\nu) \exp[-\bar{\tau}^f_{6^2S_{1/2}\to 7^2P_{1/2}}(\nu)] \mathrm{d}\nu}. \tag{25}$$

If cascade effects are negligible, we have $\tilde{k}_{7^2P_{3/2}} \approx \tilde{k}_{7^2P_{1/2}}$ for both lines (de Tomasi *et al.*[5]) and the $7P_{3/2}$ and $7P_{1/2}$ levels become approximately equally populated. It seems reasonable, at a first approximation, to assume that $\Theta_{455.5\text{ nm}}/\Theta_{459.3\text{ nm}} \approx 1$. Consequently, the retrofluorescence signal ratio is given by the relative value of the effective branching ratio of the 455.5- and 459.3-nm transitions.

The transition probabilities for Cs are known to be

$$\Gamma^e_{7^2P_{3/2}} = 8.25 \times 10^6 \text{ s}^{-1},$$

$$\Gamma^{e}_{7^2P_{3/2}\to 6^2S_{1/2}} = 2.97 \times 10^6 \ \mathrm{s}^{-1},$$

$$\Gamma^{e}_{7^2P_{1/2}} = 7.23 \times 10^6 \ \mathrm{s}^{-1},$$

$$\Gamma^{e}_{7^2P_{1/2}\to 6^2S_{1/2}} = 2.12 \times 10^6 \ \mathrm{s}^{-1},$$

and we have $\phi_{455.5\ \mathrm{nm}}/\phi_{459.3\ \mathrm{nm}} \approx 1.22$.

In Section 4 we compare the theoretical integrated signal generated by the laser energy-pooling processes with the experimental results. We must expect a retrofluorescence signal resulting from pooling processes, which gives us the same information about $\bar{\varepsilon}_{F_g}$ or $\bar{A}^{f}_{J_e\to J_g}$ as we can obtain from the direct resonance retrofluorescence at 852.2 nm. We now have an appropriate model for the investigation of retrofluorescence characteristics related to the laser energy-pooling collisions near a dissipative thin layer.

4. RETROFLUORESCENCE EXPERIMENTAL RESULTS

We divide this section into three parts: the first describes the experimental setup, the second presents measurements of a large spectral range when the laser is tuned to the edges and to the center of the 852.2-nm line, and the last presents the integrated line shapes at 455.5 and 852.2 nm when the laser frequency is scanned through the 852.2-nm resonance line.

A. Experimental Setup

The experimental setup is presented in Fig. 5. The Cs vapor is excited by a frequency-modulated beam of an Environmental Optical Sensors, Inc., laser diode (Model LCU 2001 M) with a smaller than 10-MHz bandwidth. We chose the lines of the hyperfine structure $[6^2P_{3/2}\ (F_e = 5, 4, 3) - 6^2S_{1/2}\ (F_g = 4)]$ and $[6^2P_{3/2}\ (F_e = 4, 3, 2) - 6^2S_{1/2}\ (F_g = 3)]$ at 852.2 nm. The laser carries out a frequency sweep around this bandwidth and is protected from the return signal by an isolator. A fraction of the laser beam intensity is directed through a Fabry–Pérot interferometer, which permits scaling of the spectral band explored. To maintain thermal isolation, the Pyrex Cs cell is embedded in a metallic covering, leaving only the windows open. This is placed on a Mirak thermometer (Model HP 72935) at a programmable temperature under a Pyrex cover. We obtained a uniform temperature throughout the cell. The beam is directed toward the entrance cell window at an angle of ≈2° from the normal at the surface. The frequency-modulated selective-reflection spectrum is observed with a Si photodiode. The total backward radiation (backscattered, nonresonance backscattering, and light from energy-pooling collisions), captured at an angle of ≈16° with reference to the normal, is focused onto the adjustable entrance slit of the monochromator, a (Model 5) Jarrell-Ash spectrometer equipped with a photomultiplier. The spectral retrofluorescence signal from the monochromator exit slit is amplified by a picoammeter (Keithley Instruments). The signals are then digitized and sent to the computer. The spectral sweeping step of the laser is adjustable. We limited ourselves to weak laser powers for a beam area of ≈0.014 cm^2. At higher laser powers, the retrofluorescence spectrum has spectral properties that differ from those in the linear regime. These spectral properties most likely result from complex nonlinear effects.

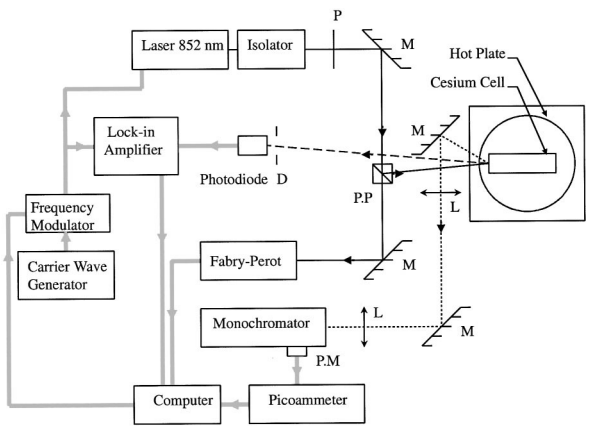

Fig. 5. Experimental setup: P, polarization rotator; L, lens; M, mirror; P.P, polarizing prism; P.M, photomultiplier; D, spatial filter.

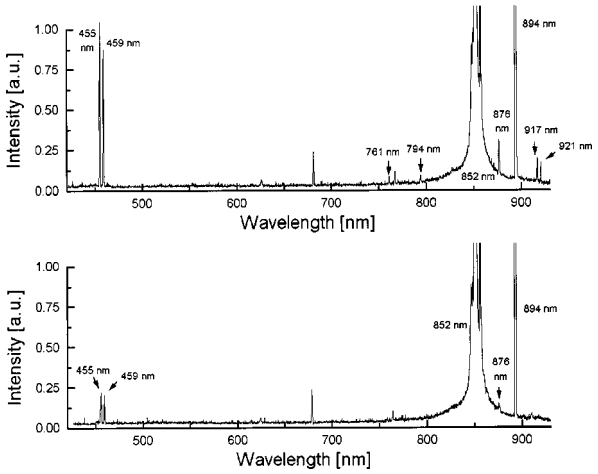

Fig. 6. Atomic retrofluorescence spectra. Top, the 852.2-nm laser tuned to the maximum of the 455.5-nm retrofluorescence signal. Bottom, the laser tuned to the center of the 455.5-nm inhibition. The temperature of the vapor was 129 °C.

B. Cesium Retrofluorescence Spectra in the 420–930-nm Spectral Range

To analyze the global influence of the nonradiative transfer of the $6^2P_{3/2}$ state energy toward the dissipative surface on the higher energy levels excited by laser energy-pooling collisions, we first investigated retrofluorescence signals over a large spectral range. The spectra shown in Fig. 6 exhibit the evolution of retrofluorescence intensity signals when the cell temperature is 130 °C. The laser power was maintained at 300 μW to ensure that the experiment operates in a linear mode. For higher laser power, the intensities of the pooling retrofluorescence lines are no longer proportional to the square of the laser power.

The spectra shown in Fig. 6 have been taken with the wavelength laser tuned at 852 nm, where we observed, the maximum and minimum intensities of the integrated retrofluorescence line at 455.5 nm. Indeed, as predicted

by theory, the spectral inhibition signature (deep dips) in retrofluorescence energy-pooling spectrum is much stronger than the inhibition observed at the 852.2-nm resonance line. So, to obtain the best information over the large spectral range, we tuned the laser as a function of the intensity of the 455.5-nm line. As predicted in Section 3, when the laser is tuned to the maximum 455.5-nm signal (top spectrum of Fig. 6), we can identify all the other lines associated with the energy-pooling collisions exciting higher levels: the 459.3-nm ($7^2P_{1/2} - 6^2S_{1/2}$) line around the same intensity as the 455.5-nm line, the 760.9-nm ($8^2S_{1/2} - 6^2P_{1/2}$) and 794.4-nm ($8^2S_{1/2} - 6^2P_{3/2}$) lines with equivalent intensity, the 894.3-nm ($6^2P_{1/2} - 6^2S_{1/2}$) line and the 876.4-nm ($6^2D_{3/2} - 6^2P_{1/2}$), 917.2-nm ($6^2D_{5/2} - 6^2P_{3/2}$), and 920.8-nm ($8^2D_{3/2} - 6^2P_{3/2}$) lines.

The second spectrum in Fig. 6 shows the same spectral range but with the laser tuned to the 852.2-nm wavelength, which corresponds to the minimum resonance retrofluorescence intensity at 455.5 nm that is in the central region of the line. We observed a drastic decrease in the intensity of all the pooling lines, which we assume to be a signature of the nonradiative transfer of the $6^2P_{3/2}$ laser-excited state toward the thin dissipative layer on the surface glass. It is worth noting that two lines (682 and 768 nm) are unaffected when the pumping laser is detuned. It seems that these lines do not correspond to the Cs atomic spectrum. In particular, the 682-nm line is too strong to be identified as the transition ($7^2F_{5/2} \rightarrow 5^2D_{3/2}$), which must have a weaker intensity. We have not identified any atomic lines compatible with these lines. They are, as well, not significantly affected

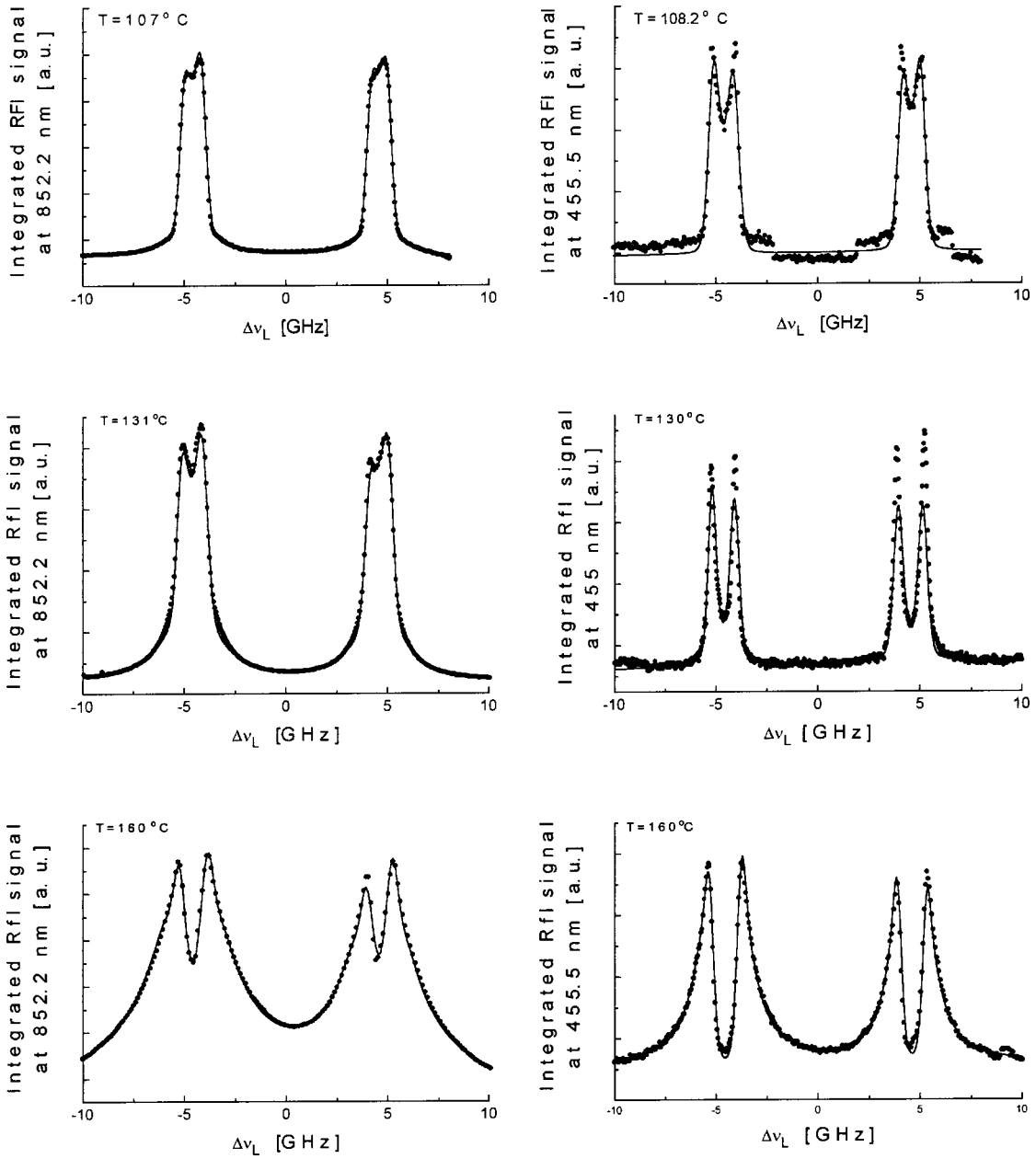

Fig. 7. Retrofluorescence signal at 852.2 nm (left column) and 455 nm (right column) as a function of laser detuning around 852.2 nm for different temperatures. Experimental results, dotted curves and theorical results, solid curves. All observations are in the linear regime.

by the cell temperature. We assume that neither is connected to the energy-pooling effect and so they are not considered in our investigation.

The 894.3-nm ($6^2P_{1/2} - 6^2S_{1/2}$) resonance line is a special case, which is known as a sensitized fluorescence. This fluorescent component has been extensively studied in the fluorescence cell at low temperatures, where its presence is caused by inelastic collisions between excited $6^2P_{3/2}$ and ground-state atoms.[9] During this excitation, internal and kinetic energies are interconnected. This excitation transfer reaction differs from the laser energy-pooling collisions. However, in our case, a preliminary study of the retrofluorescence shows that the intensity of the sensitized fluorescence line is proportional to the square of the power of the signal. Further, in the central region of this line, the inhibition effect is more of a dip than the central region of the 852.2- and 455.5-nm lines. We believe that the sensitized retrofluorescence line presents an intrinsic interest because the interaction mechanisms involved are not known in detail. The study of this line will be presented in a subsequent paper to characterize these distinctive features.

C. Integrated Retrofluorescence Spectral Lines at 455.5 and 852.2 nm as a Function of Laser Scanning Through the Resonance Line $6^2S_{1/2}(F_g) \rightarrow 6^2P_{3/2}$

Here we experimentally characterize the shapes of the 455.5- and 852.2-nm retrofluorescence lines. As indicated above, the 455.5-nm line has been selected for many reasons, principally because of its relatively high intensity even at weak pumping laser power, guaranteeing that we are operating in the linear interaction mode. Moreover, the $7^2P_{3/2}$ excited state cannot affect the population of the excited $6^2P_{3/2}$ state by spontaneous emission. In the second set of experimental measurements, the spectrometer is used as a monochromator to isolate a narrowband of the spectrum. It is at the center of the observed spectral line as the laser scans through the resonance shape of the 852.2-nm line.

Typical experimental results are shown in Fig. 7. For laser power between 20 and 500 μW, we obtained a good retrofluorescence signal in the linear regime. We show two series of experimental results for three vapor temperatures: 107 °C, 130 °C, and 160 °C. As predicted by the model, the inhibition effect within the 455.5-nm line is more pronounced than in the center of the 852.2-nm line. The maximum symmetric intensity of the 455.5-nm line signal is particularly sharp at 130 °C. The spectral properties of the 455.5-nm retrofluorescence line could easily be used for the absolute frequency stabilization of monomode lasers. It would be interesting to investigate the potential of this effect as a metrological tool and compare it with laser frequency stabilization by use of selective-reflection spectroscopy.

The preceding results lead us to consider the retrofluorescence signal related to the energy-pooling collisions as a valid way of studying processes in the boundary layer at a saturated vapor–glass surface interface. In Section 5 we consider the quantitative investigation of the theoretical and experimental behavior of the retrofluorescence signal as an optical spectroscopic method to study the dynamics of the $6^2P_{3/2}$ excited state and the energy-pooling process near a dissipative thin layer.

5. PARAMETRIC STUDY AND ANALYSIS OF THE EXPERIMENTAL RESULTS

A. Introduction

This section is devoted to the experimental investigation of the retrofluorescence signal from the interface by use of the theoretical model developed in Section 3. The main purpose of this analysis is to evaluate the effective nonradiative transfer rate $\bar{A}^f_{6^2P_{3/2}\rightarrow 6^2S_{1/2}}$ of the Cs atoms located in the near-field region. First, by using a complete parametric method we search for the minimal divergence between theoretical and experimental spectra for the 455.5-nm lines. Complementary investigations are developed when the excited hyperfine structure is disregarded. The $\bar{A}^f_{6^2P_{3/2}\rightarrow 6^2S_{1/2}}$ values extracted from the analysis of the 455.5-nm retrofluorescence signal are compared with those found when we studied the 852.2-nm resonance of the retrofluorescence signal. We conclude the section by considering the relative intensities of the 455.5- and 459.3-nm spectral lines and by providing a brief evaluation of our model of the nonresonant retrofluorescence.

B. Investigation of the 455.5- and 852.2-nm Lines with the Hyperfine Structure of the Excited State

We compare the theoretical values obtained from Eq. (20) with the experimental signals shown in Fig. 7. We assume that each hyperfine spectral line of the $6^2P_{3/2}$ fine structure has the same $\alpha^{i=l \text{ or } f}_{F_g \rightarrow F_e}(\ldots)$ profile and we regard it as a Voigt function. Nevertheless, $\alpha^i(\ldots)$ differs depending on whether atoms are in the far-field or near-field regions ($\gamma^l_{F_g} \neq \gamma^f_{F_g}$). The algorithm used to compute the fitting is based on the Levenberg–Marquardt nonlinear least-squares method as applied in the MFIT program.[10] This computer program is well suited for the parametric fitting of complex functions. The fitting results, presented as solid curves on the right-hand side of Fig. 7, are remarkably convincing. They support the model of retrofluorescence signal in the boundary layer of a metal–atomic-vapor–glass interface. To complete this analysis, we used the formalism of the resonance retrofluorescence for the 852.2-nm transition to fit these experimental results.[4] Fitted curves are shown as solid curves on the left-hand side of Fig. 7. We obtained excellent agreement between theoretical and experimental shapes for the spectral lines. The experimental quantities or parameters, which we calculated by using the fitting analysis, are listed in Table 1. The first column indicates the temperature (°C), the second, the atomic density and the third, the wavelength. Next, we present the values of the parameters defined in Section 4. We then present the most important new physical constant, $(\bar{A}^f_{6^2P_{3/2}\rightarrow 6^2S_{1/2}}/A_{6^2P_{3/2}\rightarrow 6^2S_{1/2}}) \times \bar{x}_f$ the normalized effective nonradiative transfer rate of excited atoms in the near-field layer of the Cs metallic (vapor–glass) interface, multiplied by $\bar{x}_f$ to avoid errors caused by an approximation of the mean geometric depth of the near-field region (currently defined

Table 1. Calculated Values Obtained with Hyperfine Fitting of the Characteristic Parameters[a]

T (°C)	n ($\times 10^{13}$ cm^{-3})	λ (nm)	$\bar{\varepsilon}_{F_g=4} \times \bar{x}_f$ ($\lambda_{852.2}$)	$\bar{\varepsilon}_{F_g=3} \times \bar{x}_f$ ($\lambda_{852.2}$)	$(\bar{A}^f_{J_e \to J_g}/A_{J_e \to J_g}) \times \bar{x}_f$ ($\lambda_{852.2}$)
107	2.2	455.5	86	139	109
		852.2	86	105	94
125	5.9	455.5	59	91	73
		852.2	62	72	66
130	8.0	455.5	58	72	64
		852.2	49	70	58
147	17.8	455.5	40	58	48
		852.2	32	50	40
160	32.3	455.5	30	43	36
		852.2	22	36	28

[a] For retrofluorescence signals 455.5 nm ($7^2P_{3/2} \to 6^2S_{1/2}$) and 852.2 nm ($6^2P_{3/2} \to 6^2S_{1/2}$). $\bar{x}_f$ is the effective geometric depth of near-field region, $A_{J_e \to J_g}$ and $\bar{A}^f_{J_e \to J_g}$ are the Einstein spontaneous emission rate and the effective nonradiative transfer rate in the near-field region of $6^2P_{3/2} \to 6^2S_{1/2}$, $\bar{\varepsilon}_{F_g}$ is the ratio between the effective nonradiative and radiative transfer rates for the $6^2P_{3/2} \to 6^2S_{1/2}(F_g)$ transition, and n is the atomic density.

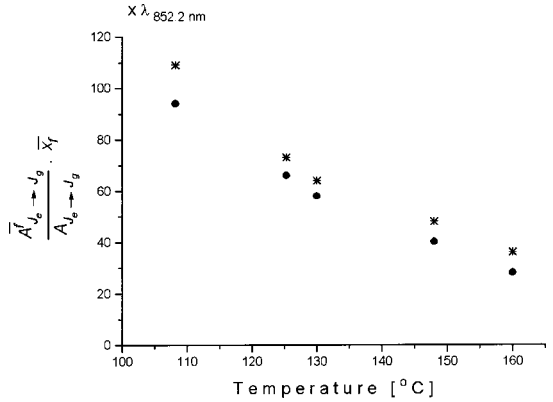

Fig. 8. Variation of the nonradiative parameter $(A^f_{J_e \to J_g}/A_{J_e \to J_g}) \times \bar{x}_f$, as a function of temperature calculated directly from the integrated resonance retrofluorescence signal at 852.2 nm (●) and from the integrated pooling-effect-induced retrofluorescence signal at 455.5 nm (*) with a hyperfine structure.

between λ and $\lambda/2\pi$). The values of the effective rates obtained from an analysis of the 455.5 or 852.2-nm lines for the same saturated vapor temperature agree relatively well, considering that the spectral lines are generated by different processes near the surface.

C. Summary of Data Analysis

The curve in Fig. 8 shows the experimental results listed in Table 1 as a function of temperature. It is seen that the sets of experimental values are not straight lines and that this quantity decreases with an increase in temperature or atomic density of the vapor. This previously observed decrement[4] can be principally associated with the screening of absorbing atoms that continually pass in and out of the boundary layer. The preceding effect, together with photon trapping and atomic quenching collisions that involve excited atoms, can contribute to a modification of Doppler broadening in the center of the spectral retrofluorescence signal.

D. Comparative Intensities of the 455.5- and 459.3-nm Lines

The large spectral range retrofluorescence signal shown in Fig. 6 permits us to evaluate directly the ratios of the integrated intensities of the retrofluorescence of the 455.5- and 459.3-nm lines. The ratio values at maximal and minimal intensities are 1.21 and 1.14, respectively. The theoretical value estimated in Section 3 is 1.22. The small discrepancy between the theoretical and the experimental ratio, less than 6.5%, confirms the validity of the hypothesis used in our model of the retrofluorescence signal.

6. DISCUSSION AND CONCLUSION

We conducted an experimental investigation using a diode laser-induced retrofluorescence method on optically thick Cs vapor in a glass cell. A diode laser with a spectral bandwidth of less than 10 MHz, tunable across the 852.2-nm Cs resonance line profile, was used to stimulate retrofluorescence. We characterized the laser-induced nonresonant retrofluorescence spectrum over the wavelength range from 420 to 930 nm. We theoretically and experimentally examined the processes that can influence the energy-pooling collisions in the vicinity of a thin dissipative surface on a glass substrate. The nonresonant backscattered laser-induced fluorescence from a dense atomic vapor has been modeled by use of the formulation of resonant retrofluorescence developed by Le Bris *et al.*[4] For the first time to our knowledge, we obtained a satisfactory quantitative interpretation of the inhibition effect (depletion) of the energy-pooling collisions and the important signature of the correlation between resonant and nonresonant spectra from the glass–metal vapor interface. The effective value of the $\bar{A}^f_{6^2P_{3/2} \to 6^2S_{1/2}}$ nonradiative transfer rate for excited Cs atoms located in the near-field region has been estimated by analysis of the 455.5-nm ($7^2P_{3/2} \to 6^2S_{1/2}$) and 852.2-nm ($6^2P_{3/2} \to 6^2S_{1/2}$) lines.

The 894.4-nm sensitized fluorescence line resulting from the ($6^2P_{1/2} \to 6^2S_{1/2}$) transition is well known from optically thin vapor. However, from our preliminary experimental observations of optically thick vapor the sensitized retrofluorescence signal seems to disagree with the predicted value from the classical reaction. We observed a strong inhibition signal that seems to be related to retrofluorescence resulting from energy-pooling processes.

This new effect in optically thick vapor is now being analyzed in our laboratory. To this end, we investigated a direct transition from the $6^2P_{3/2}$–$6^2P_{3/2}$ configuration of quasi-molecule Cs_2 near a dissipative surface to two atoms in the $6^2P_{1/2}$ excited state.

To make progress in our research on laser-induced retrofluorescence spectroscopy, it is important for us to have a quantitative theory that permits estimation of the effective $\bar{A}^f_{6^2P_{3/2}\rightarrow 6^2S_{1/2}}$ nonradiative transfer rate. How the atomic excited energy can transfer from the atom toward the film surface is also a relevant question. By using two tunable lasers for pumping at 852.2 nm and 760.9 or 794.4 nm, respectively, we provide a powerful spectroscopic method for investigating the growing population by cascade effects of the 7^2P_J levels. These effects can be monitored with the 455.5- or 459.3-nm signal intensities. It seems reasonable to assume that laser-induced retrofluorescence combined with fast modulation techniques (intensity or frequency) is a good method for investigation of laser-induced collisional avalanches in optically thick vapor. The shape of the retrofluorescence line at 455.5 nm is characterized by two narrow symmetric lines, which, therefore, appears to be a good candidate to frequency lock a diode laser that operates at 852.2 nm in the near-infrared region.

Beyond a few milliwatts of laser power, we observed the reduction of the inhibition of the 852-nm line, which we attribute to nonlinear saturation of the $6^2S_{1/2} \rightarrow 6^2P_{3/2}$ transition in the near-field region. The nonradiative transition in this region that results from the elementary transformation of photonic into thermal energy cannot produce a dip in the resonant retrofluorescence spectral line. In the nonlinear regime, we always observe an inhibition effect in the retrofluorescence spectral line that results from energy-pooling collisions; this result seems to be related to an unknown nonradiative mechanism of energy transfer in the near-field region of the interface. We await more experimental and theoretical information before reaching a conclusion on this hypothesis.

ACKNOWLEDGMENTS

This research was funded in part by the Natural Sciences and Engineering Research Council of Canada. The expert technical assistance of P. A. Dion is gratefully acknowledged. We are grateful to A. Yelon and P. Desjardins for their helpful comments.

The e-mail address for J.-M. Gagné is jmgagne @polymtl.ca.

REFERENCES

1. M. Chevrollier, M. Fichet, M. Oria, G. Rahmat, D. Bloch, and M. Ducloy, "High resolution selective reflection spectroscopy as a probe of long-range surface interaction: measurement of the surface van der Waals attraction exerted on excited Cs atoms," J. Phys. (Paris) II **2**, 631–657 (1992).
2. K. Zhao, Z. Wu, and H. M. Lai, "Optical determination of alkali metal vapor number density in the vicinity ($\sim 10^{-5}$ cm) of cell surfaces," J. Opt. Soc. Am. B **18**, 1904–1910 (2001).
3. V. G. Bordo, J. Loerke, L. Jozefowski, and H.-G. Rubahn, "Two-photon laser spectroscopy of the gas boundary layer in crossed evanescent and volume waves," Phys. Rev. A **64**, 012903/1–11 (2001).
4. K. Le Bris, J.-M. Gagné, F. Babin, and M.-C. Gagné, "Characterization of the retrofluorescence inhibition at the interface between glass and optically thick Cs vapor," J. Opt. Soc. Am. B **18**, 1701–1710 (2001).
5. F. de Tomasi, S. Milosevic, P. Verkerk, A. Fioretti, M. Allegrini, Z. J. Jabbour, and J. Huennekens, "Experimental study of caesium $6P_J + 6P_J \rightarrow 7P_{J'} + 6S$ energy pooling collisions and modelling of the excited atom density in the presence of optical pumping and radiation trapping," J. Phys. B **30**, 4991–5008 (1997).
6. R. R. Chance, A. Prock, and R. Silbey, "Comments on the classical theory of energy transfer," J. Chem. Phys. **62**, 2245–2253 (1975).
7. Z. J. Jabbour, R. K. Namiotka, J. Huennekens, M. Allegrini, S. Milosevic, and F. de Tomasi, "Energy-pooling collisions in cesium: $6P_J + 6P_J \rightarrow 6S' + (nl = 7P, 6D, 8S, 4F)$," Phys. Rev. A **54**, 1372–1384 (1996).
8. J. B. Taylor and I. Langmuir, "Vapour pressure of Caesium by the positive ion method," Phys. Rev. **51**, 753–760 (1937).
9. L. Krause, "Sensitized fluorescence and quenching," *The Excited State in Chemical Physics*, J. W. McGowan, ed. (Wiley, New York, 1975), pp. 267–316.
10. M. Zinkin, MFIT version 0.3 (1997), http://www.ill.fr/tas/matlab/.